PHILOSOPHICAL TRANSACTIONS B

royalsocietypublishing.org/journal/rstb

Research

Cite this article: Kang V, Püffel F, Labonte D. 2023 Three-dimensional kinematics of leaf-cutter ant mandibles: not all dicondylic joints are simple hinges. *Phil. Trans. R. Soc. B* **378**: 20220546.
https://doi.org/10.1098/rstb.2022.0546

Received: 12 April 2023
Accepted: 15 July 2023

One contribution of 18 to a theme issue 'Food processing and nutritional assimilation in animals'.

Subject Areas:
biomechanics, evolution

Keywords:
mastication, chewing, jaws, instantaneous helical axis, instantaneous rotational axis, joint degrees of freedom

Author for correspondence:
David Labonte
e-mail: d.labonte@imperial.ac.uk

†Joint first authors.

Electronic supplementary material is available online at https://doi.org/10.6084/m9.figshare.c.6834890.

THE ROYAL SOCIETY PUBLISHING

Three-dimensional kinematics of leaf-cutter ant mandibles: not all dicondylic joints are simple hinges

Victor Kang†, Frederik Püffel† and David Labonte

Department of Bioengineering, Imperial College London, London SW7 2AZ, UK

VK, 0000-0003-0959-1364; FP, 0000-0002-3917-0942; DL, 0000-0002-1952-8732

Insects use their mandibles for a variety of tasks, including food processing, material transport, nest building, brood care, and fighting. Despite this functional diversity, mandible motion is typically thought to be constrained to rotation about a single fixed axis. Here, we conduct a direct quantitative test of this 'hinge joint hypothesis' in a species that uses its mandibles for a wide range of tasks: *Atta vollenweideri* leaf-cutter ants. Mandible movements from live restrained ants were reconstructed in three dimensions using a multi-camera rig. Rigid body kinematic analyses revealed strong evidence that mandible movement occupies a kinematic space that requires more than one rotational degree of freedom: at large opening angles, mandible motion is dominated by yaw. But at small opening angles, mandibles both yaw and pitch. The combination of yaw and pitch allows mandibles to 'criss-cross': either mandible can be on top when mandibles are closed. We observed criss-crossing in freely cutting ants, suggesting that it is functionally important. Combined with recent reports on the diversity of joint articulations in other insects, our results show that insect mandible kinematics are more diverse than traditionally assumed, and thus worthy of further detailed investigation.

This article is part of the theme issue 'Food processing and nutritional assimilation in animals'.

1. Introduction

Jaws are an important evolutionary innovation in vertebrates, and show a remarkable diversity in both morphology and kinematics (e.g. [1]). As illustrative examples, jaws in some teleost fish are integrated with other skeletal elements to render their skull into a complex multi-bar linkage [2]; mammals characteristically combine jaw translation and multi-axis rotation into complex chewing movements (e.g. [3–9]); and stingrays, salamanders and some carps have convergently evolved jaw kinematics that resemble those observed in mammals [10–13]. The rich diversity and significance of jaw kinematics in vertebrates is reflected in the array of advanced quantitative techniques used to study them, including three-dimensional (3D) motion capture, X-ray reconstruction of moving morphology (XROMM), neural-network assisted automatic tracking and rigid body mechanics (e.g. [9,14–17]).

By contrast, our quantitative and functional understanding of mandible movements in hexapods is nascent (e.g. [18,19]). This discrepancy is partly due to the experimental difficulties associated with capturing and digitizing the motion of small and often fast-moving mandibles, and partly due to the need for high-resolution 3D imaging techniques such as laboratory-based computed micro-tomography, which have only recently become more accessible and widely used. Consequently, current perspectives on hexapod mandibular function have focused on comparative morphology, qualitative *in vivo* observations, or detailed analyses of the evolutionary history of mandible

morphology [20]. In the earliest hexapod lineages—the coneheads (Protura), springtails (Collembola) and two-pronged bristletails (Diplura)—mandibles have a single articulation point [21], and are actuated by multiple muscle groups [22–25]. However, in Dicondylia, a taxonomic group encompassing most extant insect species, the morphology of the mandible–head complex is markedly different: load-bearing structures of the head-capsules are strengthened [22,26], mandibles articulate via two distinct condyles, and are typically actuated by only one antagonistic pair of muscles [24,25,27–31]. Most of the winged biting–chewing insects studied to date, including dragonflies [32], cockroaches [33] and beetles [34,35], have such dicondylic joints characterized by two prominent mandibular condyles. Indeed, the transition from monocondylic to dicondylic mandibles is considered a pivotal moment in insect evolution (e.g. [23,36,37]), paralleling the rise of jawed fish in early vertebrate evolution: it is thought to be associated with an increase in bite forces, and may have afforded early insects access to a wider range of food sources [22,25,37].

Another consequence of the emergence of dicondylic mandible joints is a putative simplification of possible mandible motion. A single condyle that articulates like a ball-and-socket joint allows three rotational degrees of freedom (DoF). Two condyles, in turn, can form two ball-and-socket joints, which are then thought to constrain mandible motion to rotation about a virtual axis that connects their centres (e.g. [24,25,31,33]). Mandible joints of winged insects with biting–chewing mouthparts (Odonata and Neoptera) are thus classified as obligate dicondylic [25]—they are simple one DoF hinge joints that only permit rotation about a single fixed axis. In light of the staggering diversity and complexity of jaw movements in vertebrates, the alleged conformity to a simple hinge joint in the mandibles of the most speciose animal taxon may raise curious eyebrows. During the last 400 Myr, insect mouthparts have undergone multiple independent and stunningly complex evolutionary modifications: to give but two examples, in many hemipteran and dipteran species, biting mouthparts have been adapted into stylets for piercing, while in other Dicondylia, dicondylic joints have undergone a secondary reduction to monocondyly [20,30,31,38]. Is it really plausible that all dicondylic mandibles of winged biting insects are adequately described by the same hinge joint paradigm? Although restriction to a single DoF simplifies neuromechanical control and may increase net bite force by channelling muscle force into two antagonistic muscle pairs [33,35,39–41], it is not free from disadvantages. In mammals, for example, multiple jaw DoFs enable an array of masticatory kinematics, with significant benefits to the ability to nutritionally process food (e.g. [42,43]). Although many dicondylic mandibles possess regions that are ascribed a 'grinding function' and likened to mammalian molars (e.g. [21,24,44–48]), it would appear that two mandibles rotating about hinge joints are somewhat ill-suited for effective grinding, which requires relative motion between two surfaces that are pressed together.

Perhaps surprisingly, there is no quantitative evidence in support of the widespread idea that the kinematics of dicondylic mandibles in winged biting insects can be described by a single rotational DoF. One may argue that it is hard to imagine how a joint with two conspicuous condyles could depart from rotation about the axis they define. But few, if any, well-developed condyles form perfect ball-and-socket joints, and not all putatively dicondylic mandibles have two well-developed condyles. Indeed, recent work has revealed some cracks in the surface of the canonical assumption that all mandibles of winged biting insects rotate about a single fixed axis. Gronenberg *et al.* [49], for example, inferred from high-speed video observations that mandible movements in a trap-jaw ant are suggestive of a mechanical 'cam' within the joint, which is crucial for the successful preparation of a mandible strike. This cam is formed by protrusions on the head-capsule, which guide a supposed sliding motion of the mandibular stem. Zhang *et al.* [50–52] studied mandible kinematics in a ponerine ant, and suggested that bi-axial rotation of mandibles can confer multifunctionality: at small opening angles, ants can grasp delicate objects with concavities located on the ventral section of the mandible, but owing to slight mandible roll, they can also cut and pierce prey with sharp teeth on the dorsal side when opening angles are large. In several detailed studies on formicoid head morphology, it was noted that ant mandible joints may depart from a strict obligate dicondylic morphology, and instead have reduced or otherwise altered articulations ([53–55], see also [56]). Using anatomical inference, computational visualizations and experiments with 3D printed models to indirectly infer mandible kinematics, it was suggested that here, too, the leading assumption of a simple hinge joint breaks down [53,55]. Evidence for more complex articulation morphology is not restricted to ants: mandibles of parasitoid chalcid wasps appear to have reverted to 'secondary monocondyly' to re-access DoFs that had been made unavailable by dicondylic joints [31].

Common to these studies is their use of morphological inference and qualitative observations as supporting evidence. Quantitative analyses of joint DoFs using rigid body mechanics, which are widely applied in vertebrates, are rarely used in insects (e.g. [57]). In this study, we address this gap, and use both qualitative and quantitative methods to characterize the mandible motion in *Atta vollenweideri* Forel, 1893 leaf-cutter ants. Leaf-cutter ants harvest plant fragments to cultivate a specialized fungus that serves as the primary food source for the colony [58,59]. They forage on a wide range of plant materials, including leaves, flowers and fruit of varying physical properties [60,61]. Thus, leaf-cutter ants use their mandibles to bite and cut through materials that can be soft, hard, tough, thin or thick, in addition to carrying out a variety of other tasks, such as brood care, material transport and nest building. We used marker-based motion capture to reconstruct mandibular motion of *A. vollenweideri* ants in 3D and *in vivo*, and then analysed the data using rigid body mechanics to investigate whether the observed kinematics are consistent with a simple hinge joint. These quantitative analyses are supplemented with descriptions of joint morphology, and observations of mandible movements during unrestrained cutting and biting, to provide a comprehensive account of mandible joint function.

2. Methods

(a) Study animals

A colony of *A. vollenweideri* leaf-cutter ants, founded and collected in Uruguay in 2014, was used for all experiments. The colony was kept inside a climate-controlled chamber (Fito-Clima 12.000 PH, Aralab, Rio de Mouro, Portugal), on a 12/12

h day/night cycle at 25°C and 60% relative humidity. It had access to leaves of bramble, laurel and kibbled maize ad libitum, regularly provided in two foraging boxes connected to the colony via plastic tubing.

(b) Behavioural observations, manual mandible manipulation and scanning electron microscopy

Ant workers cutting either bramble leaves or polydimethylsiloxane polymer films (PDMS; approximate thickness: 300 µm) were video-recorded using a Raspberry Pi High Quality camera (Raspberry Pi Foundation, Cambridge, UK), equipped with a 25 mm C-mount lens (LM25JC, Kowa Optimed Deutschland, Düsseldorf, Germany), and controlled via a Raspberry Pi model 3B. For observations of mandible movements at higher magnifications, individual worker ants were secured in a 3D printed mount and recorded under a stereomicroscope (Z6, Leica Microsystems, Wetzlar, Germany). Thick mid-veins of bramble leaves were offered to the worker ants to observe mandible movements during cutting.

Three mature workers, between 19 and 20 mg in body mass, were selected from the foraging box connected to the colony, and sacrificed by freezing. Immediately after isolating the ant head using a scalpel, the mandibles were carefully manipulated under a stereomicroscope (S Apo, Leica Microsystems, Wetzlar, Germany), to qualitatively assess their range of motion. The head-capsule was held with tweezers, and a second pair of tweezers was used to gently push the right mandible downwards as both mandibles were fully closed. One manipulation trial was filmed with a smartphone through the eye-piece of the stereomicroscope (Google Pixel 6a, 1920 × 1080 pixels, 30 frames per second (fps)).

Following manual manipulation, one of the three head samples was halved using a scalpel. The left hemisphere was left intact, but the mandible from the right hemisphere was removed by holding it near the distal end with tweezers. All samples were air-dried in a desiccator for 4 days, and then mounted on aluminium stubs, using carbon tape and silver conductive paint, to prepare them for scanning electron microscopy (SEM). The specimens were sputter-coated with approximately 30 nm of gold (Emitech K575X, Quorum Technologies, Laughton, UK), and imaged in secondary electron mode using a tungsten filament SEM (JSM-6010LA, JEOL, Tokyo, Japan).

(c) Multi-camera rig for 3D motion tracking

To characterize *in vivo* mandible motion in 3D, a multi-camera recording rig was constructed with 30 × 30 mm aluminium struts and 3D printed joineries (figure 1*a*). Four CMOS USB cameras (2× model DMK 33UX265, 2× DMK 33UX252; The Imaging Source Europe, Bremen, Germany), each equipped with a Telecentric lens (Computar TEC-M55, CBC America, NC, USA), were mounted on this rig via custom-designed camera mounts with five DoFs, which helped to adjust camera orientation and lens focus. The object of interest—either a live specimen or a calibration target—was first mounted on a 3D printed platform, which was then slotted into a 3D printed stage with three DoFs, used to position the sample within the field of view of the cameras. The scene was illuminated with LED lamps (LED desk lamp, IKEA, Delft, The Netherlands), and the cameras were synchronized using a custom-built external trigger comprising an Arduino Nano microprocessor, programmed to send pulse signals to the trigger port of each camera in parallel. Synchronized images were captured at 60 fps with a resolution of 2048 × 1536 pixels, using the software provided by the camera manufacturer (IC Capture v. 2.5.1547.4007, The Imaging Source).

A 1 × 1 LEGO plate was used as calibration target, a common choice for 2D and 3D calibration owing to LEGO's strict manufacturing standards (e.g. [62,63]). Real-world distances between nine landmarks on the calibration target were measured with a digital micrometer (model 293-795-30, Mitutoyo Corporation, Sakado, Japan; maximum permissible error ±2 µm). Synchronized images of the target were then taken on all four cameras. The images were loaded into a MATLAB (R2021b, v9.10.0; MathWorks, Natwick, MA, USA) application to estimate the direct linear transformation (DLT) coefficients for camera calibration [64], which requires identification of at least six landmarks; all visible landmarks from the calibration object ($n = 9$ total landmarks) were identified from each of the four camera views. The camera calibration was validated ahead of every experimental trial involving a re-positioning or a new specimen: the current calibration was loaded into DLTdv8a [64,65], along with a short image sequence from each of the four camera views. The location of the apical tooth tip of the left mandible was selected in one random playback window, and the corresponding 2D projection line was inspected in the three remaining views. If the 2D projection lines passed through the tooth tip of each camera view, the same location was selected in a second playback window, which then returned the 3D projection and the DLT residuals. A system was considered well-calibrated if the DLT residuals were below 1.0 pixels; otherwise, it was redone.

(d) Video recording, tracking and 3D reconstruction

For each trial, one *A. vollenweideri* worker was selected from the foraging box. We selected six ants within a narrow body mass range to minimize potential size effects (20.4–23.6 mg). Each ant was positioned on a custom 3D printed mount which featured a clamp, designed to physically restrain the head-capsule during the recordings. The mounted specimen was chilled on an ice block for 1–2 min to reduce activity during subsequent marker placement. Markers were added to enable consistent and accurate tracking, using a small insect pin dipped in correction fluid (Tipp-Ex Rapid, Société Bic, Paris, France). Two constraints informed marker placement: (1) to increase the accuracy of downstream kinematic analyses, the marker positions needed to be far away from each other and yield non-collinear line elements, at least one of which is approximately perpendicular to a perceived dominant axis of rotation (see below); (2) markers needed to remain visible on at least three cameras throughout the movement. Markers were added to the second and last tooth (defined as most proximal), as well as at a coordinate near the mid-point of the mandible, opposite to the masticatory margin of the left mandible (figure 1*a*,*c*,*d*). The mounted and marked ant was kept on the ice block until the set-up was ready for acquisition; this helped to reduce active mandible movements during the wait period, which often led to loss of the markers via mandible scraping. Preliminary trials indicated that the brief cooling period had no discernible impact on subsequent behaviour. Some ants readily displayed biting movements, so the cameras were triggered, and around 2000–3000 frames were captured (corresponding to 30–50 s recording time); otherwise, individuals were encouraged to move their mandibles by a gentle puff of air. Ants used for the trials were released back to the foraging box after filming was completed.

All recordings contained multiple mandible movement sequences, and were reviewed post-trial in ImageJ v. 1.53j [66]. Frame sequences that contained mandible movements were exported and loaded into DLTdv8a [64], along with the calibration file, for marker tracking. Six landmarks were manually located on each frame: one on the approximated volumetric centre of each eye, one halfway between the ventral mandibular articulation (vma) and the atala (ala), to approximate the mandible joint location (morphological terms as per [67]), and three points on the marked mandible as described above. The output of the tracking was a 3D position vector for each landmark per frame.

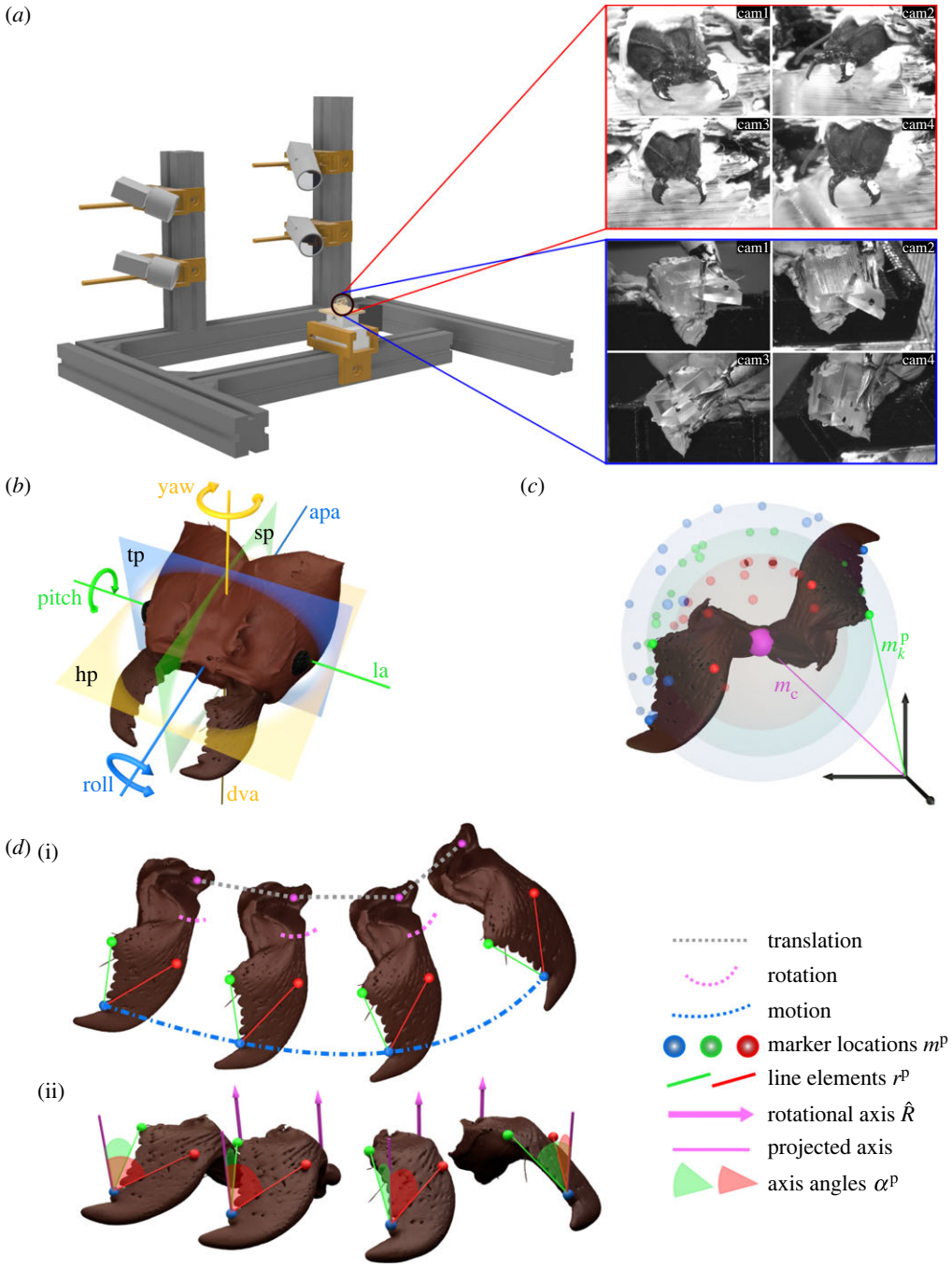

Figure 1. 3D motion capture and principles of quantitative kinematic analysis of mandible motion in *Atta vollenweideri* leaf-cutter ants. (*a*) A four-camera recording rig, built from aluminium struts and 3D printed joineries, was used to record mandible motion in 3D. Individual ants were restrained on a moveable holder (black circle), and direct linear transformation coefficients were estimated for 3D reconstruction. Top red inset: example views of a live restrained worker ant. Three markers on each mandible were used for tracking, and are visible as white spots: one distal (blue sphere in (*c*,*d*)), one intermediate (red sphere in (*c*,*d*)) and one proximal (green sphere in (*c*,*d*)). Bottom blue inset: example views of a physical hinge joint model—built from 3D printed parts and an insect pin—used as a reference for quantitative analyses. (*b*) Schematic of an *A. vollenweideri* head-capsule defining three principal planes—sagittal (sp), transverse (tp) and horizontal (hp); three principal axes—dorso-ventral (dva), anterior–posterior (apa) and lateral (la); and three principal rotations—pitch, yaw and roll. The hypothesis that *Atta* mandible joints are hinges was tested in two steps. (*c*) First, if mandibles rotate about a fixed point (pink), then all markers trace surfaces of concentric spheres. The location of the best joint centre, $\boldsymbol{m}_c$, was thus estimated by minimizing the variation of the distances between all three marker locations $\boldsymbol{m}_k^p$ and the joint centre across all frames (see equation (2.2)). For a hinge joint, this distance variation must be negligible. ((*d*(i)) Second and in general, mandible kinematics are fully captured via the combination of joint centre translation and rotation around that joint centre. (*d*(ii)) If mandibles rotate about an axis with fixed orientation, then any line element connecting two points on the mandible spans a constant angle to this axis throughout the rotation, independent of joint centre translation. The orientation of a best continuous axis of rotation (bCAR) ($\hat{\boldsymbol{R}}$, pink) was thus estimated by minimizing the variation of the angles α^p spanned by it and two mandible-fixed line elements $\boldsymbol{r}^p$ across all frames (red and green lines and angles, see equation (2.3) and main text for details). For a hinge joint, the difference between the predicted and observed angles should be close to zero, and uncorrelated, continuous, independent and normally distributed with respect to the angle of rotation about $\hat{\boldsymbol{R}}$.

(e) Kinematic analysis

The extracted position vectors were used for 3D kinematic analyses, with the aim to test the hypothesis that mandibles of leaf-cutter ants are connected to the head via hinge joints, and thus rotate about a single axis fixed both in location and in orientation. Characterization of 3D joint kinematics is a common aim

in skeletal biomechanics, and particularly in human medicine and sports science (e.g. [68–72]). In classic rigid body kinematics, a general analysis would proceed by first characterizing the orientation and then the location of an instantaneous helical axis (IHA)—the axis about which the body rotates and along which it translates at a given instant. The orientation of the IHA can be calculated exactly, through use of the rigid body constraint: all relative motion between two points on the same rigid body is due to rotation, and all points on the body share the same instantaneous angular velocity vector, $\boldsymbol{\omega}$; by definition, $\boldsymbol{\omega}$ has the same orientation as the IHA ([73], throughout this manuscript, we denote vectors as bold; unit vectors are indicated with a hat, as in $\hat{\boldsymbol{R}}$ for a unit vector in the direction of the vector $\mathbf{R}$). Three non-collinear points, A, B and C, on the rigid body then suffice to determine $\boldsymbol{\omega}$ via a direct vector solution of a set of two simultaneous equations, which reads [68]:

$$\boldsymbol{\omega} = \frac{\boldsymbol{v}_{\mathrm{B/A}} \times \boldsymbol{v}_{\mathrm{C/A}}}{\boldsymbol{v}_{\mathrm{B/A}} \cdot \boldsymbol{r}_{\mathrm{C/A}}}, \tag{2.1}$$

where $\boldsymbol{v}_{\mathrm{B/A}}$, $\boldsymbol{v}_{\mathrm{C/A}}$ and $\boldsymbol{r}_{\mathrm{C/A}}$ are the instantaneous relative velocity and relative position vectors for points A, B and C, respectively. The location of the IHA can then be found relative to any reference point X on the body via an expression that again involves the angular velocity and the instantaneous linear velocity of point X [73]. This two-step process is both theoretically exact and general, and is consequently widely used (e.g. [72,74–79]).

In principle, rotational joint DoFs can then be inferred by inspecting the temporal variation of the orientation and location of the IHA throughout a motion sequence. For a hinge joint, for example, the IHA degenerates to a single rotational axis with constant orientation and location. However, the instantaneous relative and absolute velocity vectors, required to estimate the orientation and location of the IHA, are generally unknown, and thus need to be approximated via the average relative velocities over a finite time, equal to the instantaneous velocities only in the limit of an infinitesimal time step (see e.g. [75] for a more detailed discussion). This approximation introduces a direct competition between two needs: the time step between two measurements needs to be as small as possible, so that the average velocity vectors approach the instantaneous velocity vectors; but it needs to be large enough to avoid vanishing signal-to-noise ratios. The strength of equation (2.1) is thus also its weakness: because it is an exact vector solution, any noise is necessarily interpreted as a change in the orientation and location of the IHA.

The sensitivity of the IHA to noise is a well-known problem, and can be so severe that determination of its orientation and location can be prohibitively inaccurate, even for the much simpler case of planar motion, where it reduces to an instantaneous axis of rotation (e.g. [69,75,80]). Indeed, even relatively small noise can reduce the estimate obtained through equation (2.1) to no better than a random guess (see electronic supplementary material, figure S1). To overcome this difficulty, numerous alternative methods have been proposed. These methods may be broadly split into one of two categories: the orientation of the IHA is still obtained through determination of the angular velocity vector, but filtering or other optimization routines are deployed to reduce noise (e.g. [69,75,80]); or finite difference approximations are avoided altogether, and a representative axis is estimated through minimization of cost functions that allow absorption of experimental uncertainty into an error term (e.g. [71,77,81–83]). Although these methods can reduce the sensitivity to noise, they are typically restricted to rotation about a fixed point or axis [77,81]. Other approaches exist, including some that allow joint axes' translation (e.g. [74,82,83]), but a comprehensive account of these methods and a rational comparison of their individual merits and shortcomings are beyond the scope of this study.

Because leaf-cutter ant mandibles are small (length of about 1.8 mm), we anticipated that even best-case signal-to-noise ratios may be such that direct calculation of the angular velocity vector would yield noise-ridden estimates of the IHA, preventing robust conclusions on rotational joint DoFs through inspection of its temporal variation. In order to conduct a direct test of the hinge joint hypothesis in *Atta* mandibles, we instead developed a method that leverages the advantages of cost functions, but can estimate the orientation of the rotational axis independent of joint translation. The general idea is to estimate the axis with fixed orientation and location that describes as much of the observed kinematics as possible—we will call this axis the best continous axis of rotation, or bCAR. The hypothesis of a dicondylic hinge joint will then be assessed quantitatively by statistical comparison of the explained versus observed mandible kinematics.

In order to estimate the location of the bCAR, we define a cost function that minimizes the variation of the distance between the location of P markers, $\boldsymbol{m}_k^{\mathrm{P}}$, and the best joint centre of rotation, $\boldsymbol{m}_{\mathrm{c}}$, across N frames (see [81]):

$$C_{\mathrm{L}} = \sum_{p=1}^{P} \sum_{k=1}^{N} [(\boldsymbol{m}_k^{\mathrm{P}} - \boldsymbol{m}_{\mathrm{c}})^2 - (D^p)^2]^2. \tag{2.2}$$

Here, D^{P} are the average distances between each $\boldsymbol{m}^{\mathrm{P}}$ and $\boldsymbol{m}_{\mathrm{c}}$ across all frames. If the mandible rotates about a fixed point, then all markers populate the surfaces of concentric spheres with radii D^{P}, and minimization of equation (2.2) yields the coordinate of their shared centre (figure 1*c*, see [81] for a more detailed discussion). However, a unique solution exists only if rotation occurs about more than one axis; if rotation is constrained to a single axis of rotation, *any* point on it minimizes equation (2.2), because all points now populate the circumference of concentric circles. In order to obtain a point that is biologically meaningful, we thus restricted the possible coordinate of $\boldsymbol{m}_{\mathrm{c}}$ such that it falls within a square bounding box with a side length of 20% of the distance between both eye centres (about 600 µm), around the putative joint centre (see above).

In order to determine the orientation of the rotational axis, $\hat{\boldsymbol{R}}$, we introduce the elemental geometric notion that the angle between two Euclidean vectors, $\boldsymbol{r}$ and $\hat{\boldsymbol{R}}$, can be defined via their dot product as $\cos\alpha = \boldsymbol{r} \cdot \hat{\boldsymbol{R}}/|\boldsymbol{r}|$—the basis of the widely used Rodrigues rotation formula [84]. Let $\boldsymbol{r}$ be an arbitrary vector that connects two points on a rigid body, and let this body rotate by a movement angle θ about an axis with fixed orientation $\hat{\boldsymbol{R}}$. The angle α, and thus $\boldsymbol{r} \cdot \hat{\boldsymbol{R}}$, remain constant throughout the rotation. More generally, any line element $\boldsymbol{r}^{\mathrm{P}}$ that connects two points on a rigid body forms a constant angle α^{P} to $\hat{\boldsymbol{R}}$ throughout any rotation about $\hat{\boldsymbol{R}}$ (figure 1*d*). Crucially, this angle is invariant to translation of either the body or the rotational axis. $\hat{\boldsymbol{R}}$ can thus be estimated via a cost function that minimizes the variation of α^{P} for $P-1$ independent vectors spanned by P markers across N frames:

$$C_{\mathrm{o}} = \sum_{\mathrm{p}=1}^{P-1} \sum_{k=1}^{N} [\alpha_k^{\mathrm{P}} - \overline{\alpha}^{\mathrm{P}}]^2, \tag{2.3}$$

where α_k^{P} is the angle between $\boldsymbol{r}_k^{\mathrm{P}}$ and $\hat{\boldsymbol{R}}$ at the kth time instant, and $\overline{\alpha}^p$ is the arithmetic mean angle for each vector:

$$\overline{\alpha}^{\mathrm{P}} = \frac{1}{N} \sum_{k=1}^{\mathrm{N}} \alpha_k^{\mathrm{P}} = \frac{1}{N} \sum_{k=1}^{\mathrm{N}} \arccos\left[\hat{\boldsymbol{R}} \cdot \frac{\boldsymbol{r}_k^{\mathrm{P}}}{|\boldsymbol{r}_k^{\mathrm{P}}|}\right]. \tag{2.4}$$

In a sense, the cost function defined by equation (2.3) is a reformulation of equation (2.1), with the key difference that it can consider data from an arbitrary number of line elements to fit a single axis to an arbitrary number of observations, as opposed to determination of one single solution per point pair via a finite difference approximation. Thus, for $P = 3$ markers

and $N = 2$ frames close in time, minimization of equation (2.3) yields an estimate for the orientation of the IHA; but in practice, it is then subject to similar trade-offs to those laid out above (see electronic supplementary material for a more detailed performance evaluation).

To apply equation (2.3) to our experimental data, we defined two line elements $\boldsymbol{r}^{\mathrm{P}}$ for each mandible, as the vectors connecting the most distal marker to the other two markers. All 3D kinematics data per individual were then subjected to the cost function defined by equation (2.3) to determine the orientation of the bCAR per individual.

(f) Statistical assessment of the hinge joint hypothesis

In order to test how well mandible kinematics can be described as rotation about a fixed point, we assessed the variation of the distance between $\boldsymbol{m}^{\mathrm{P}}$ and $\boldsymbol{m}_{\mathrm{c}}$ across all recorded frames per individual. The magnitude of this variation was then assessed by comparing it with (i) the accuracy of the distance measurements on the calibration target (±2 µm, see above); (ii) the size of one image pixel (7 µm); (iii) the lengths of the mandible (about 1.8 mm) and of the effective mandible in-lever (about 600 µm, see [41]); and (iv) the variation obtained for a physical model hinge joint (see below and figure 1*a*).

To test whether mandible kinematics can be accurately described as rotation about an axis with fixed orientation, we extracted the residuals resulting from the minimization of equation (2.3)—the difference between expected and observed angles α_k^{P}—and then inspected their distribution across the movement angle range $\theta_{\max}$. The movement angle range $\theta_{\max}$ was defined as the largest angle that was spanned between all vectors that connect the bCAR, located through equation (2.2), with the most distal marker in the plane of rotation. If mandible motion is restricted to rotation about a single axis with fixed location and orientation, these residuals should be small, continuous, independent and normally distributed with respect to the movement angle θ; θ can be defined with respect to any reference vector that connects the bCAR to the most distal marker in the plane of rotation, and we defined it such that it is zero when mandibles were fully opened. To formally assess these necessary statistical conditions, we conducted an ordinary least squares regression between residuals and movement angle θ, and then subjected the residuals to the Global Validation of Linear Models Assumptions test developed by Peña & Slate [85], implemented in the R-package *gvlma*, using the global test statistic with a significance level of 0.05. The null hypothesis of rotation about an axis with fixed orientation was retained only if there was no significant relationship between the residuals and movement angle, and if the linear model assumptions were met. Two further parameters were extracted as proxies for the quality of fit: the standard deviation of the residuals resulting from minimization of the cost function (averaged across both line elements); and the ratio between the observed and predicted distance moved by the mandible, from here on referred to as distance metric. The observed distance is the total distance covered by the individual markers; the predicted distance is the sum of distances between the marker locations projected onto the plane of rotation.

In order to compare results across ants, we converted individual-specific movement angles into global opening angles independent of the orientation of the rotational axis; we defined the opening angle as the angle spanned by the vector that connects the joint centre with the most distal tracking point and the normal of the sagittal plane (figure1*b*). All kinematic calculations were conducted in Python v. 3.9.13, and all statistical analyses were conducted in R v. 4.1.2. All data reported in the text correspond to mean ± standard deviation unless otherwise indicated.

(g) Validation

In order to validate the experimental and analytical methods, we tested them on experimental data obtained from a well-defined physical model with a hinge joint (inset in figure 1*a*). The model, consisting of a 'head-capsule' and a 'mandible', was designed in Autodesk Fusion 360 (Autodesk, San Rafael, CA, USA) to have similar dimensions to a 20 mg worker ant head-capsule and mandible, and was printed using a stereolithography resin printer (Form3, Formlabs, Somerville, MA, USA). The mandible was held in place within the head-capsule by an insect pin that served as rotational axis; rotation about this axis was induced with a gentle push from a fine-tip paintbrush ($n = 3$ instances from one model). The resulting movement was recorded using the set-up described above, and the 3D coordinates of the following landmarks were extracted for each frame: three points on the mandible (one distal, one intermediate, one proximal); two points on the longitudinal axis of the insect pin to serve as the ground truth rotational axis; and two points on the head-capsule to define a horizontal vector orthogonal to the rotational axis. The data were then subjected to the same analysis as described above to estimate the error associated with the 3D reconstruction and tracking, and the accuracy of the rigid body kinematic analysis.

(h) Computed micro-tomography and 3D visualization

3D printed models and computer animations were used to intuitively explore and visualize mandible kinematics (see also [55]). To this end, we used a computed micro-tomography scan of an *A. vollenweideri* worker with a body mass of 23.7 mg, obtained for a previous study [86], and similar in body mass to the workers investigated herein. The surface meshes of mandibles and head-capsule, segmented previously in ITK-SNAP [86], were exported out of ITK-SNAP as OBJ files and decimated using the 'quadratic edge collapse simplification' function in MeshLab v. 2020.03 [87]. After further cleaning in MeshLab, the meshes were imported into Blender v. 2.91.0, and the mandibular motion was visualized based on either (i) the real-world tracked points or (ii) the bCAR and the opening angle derived from the same points, using data from a representative worker of similar body mass (21.1 mg).

3. Results

(a) Mandible joint morphology

The mandible interfaces with the head-capsule via the mandible stem. The stem bears the ventral mandibular articulation (vma), the atala (ala) and the dorsal mandibular articulation (dma), which together define the joint (figure 2*a*). The vma and ala resemble ball-and-socket joints; the dma, in contrast, is elongated and akin to a hinge (figure 2*a*,*b*). The cuticular surface of the ala is partially covered in a dense field of short spine-like protuberances, which terminate in either a single peak or multiple peaks (figure 2*a*(iii)). A region of the ala surface that is microscopically smooth and completely devoid of protuberances is exposed when the mandible is fully closed (figure 2*a*(ii,iii)). Long slender hairs are present on the lower (ventral) half of the ala, but not on its dorsal half (figure 2*a*(iii)). Both the vma and the dma cuticular surfaces lack the spine-like protuberances. The slender hairs are present, but with lower density (figure 2*a*(iii)).

(b) Qualitative observations of mandible kinematics during cutting and biting

When cutting bramble leaf lamina, *A. vollenweideri* worker ants draw their mandibles from approximately fully open to

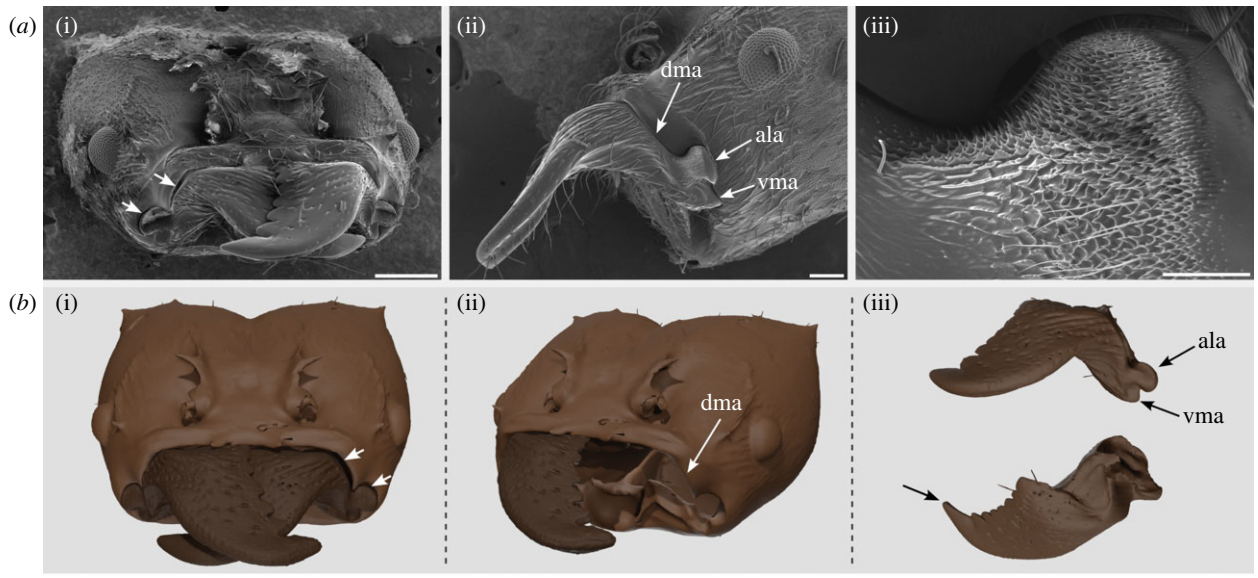

Figure 2. Morphology and kinematics of *Atta vollenweideri* leaf-cutter ant mandibles. (*a*(i)) Scanning electron microscopy image of a worker ant head-capsule. When the mandibles are closed, there is a discernible gap between the head-capsule and the dorsal articulation of the inferior mandible (white arrows), noticeably larger than the gap in the same region of the superior mandible. Scale bar: 0.5 mm. (*a*(ii)) Lateral view of the head-capsule, the left mandible and the mandible joint. The joint morphology is defined by the dorsal mandibular articulation (dma), the atala (ala) and the ventral mandibular articulation (vma). Scale bar: 0.2 mm. (*a*(iii)) The surface of the ala is covered in spine-like protrusions and hairs. The surfaces of the dma and vma are smooth. Scale bar: 0.05 mm. (*b*(i)) 3D rendering of the head-capsule and left mandible of a different *A. vollenweideri* specimen, generated from computed micro-tomography images (false colours). White arrows indicate the gap between the inferior left mandible and the dma, also evident in (*a*(i)). (*b*(ii)) An ant head-capsule was digitally dissected to remove the left mandible and muscles. The dma is elongated and distinct in shape from the vma and ala. (*b*(iii)) Lateral and dorsal views of the left mandible (top and bottom, respectively). The arrow marks the apical tooth on the masticatory margin.

almost fully closed. This motion visually resembles transverse adduction (figure 3*a* and electronic supplementary material, video SV1). Mandibles were sometimes closed sufficiently to overlap, in particular when cuts were initiated at the free leaf edge, or when workers attempted to cut thick leaf veins (figure 3*b* and electronic supplementary material, video, SV2). Notably, there was no apparent pattern of preference for either the left or right mandible ending up as superior. Indeed, we observed swaps in superiority during *in vivo* cutting of thick leaf veins, leaf lamina and thin PDMS films (figure 3*b* and electronic supplementary material, videos SV2 and SV7). That both the left and right mandible can be superior suggests that the kinematic space accessible to the mandibles may not be limited to rotation about a fixed axis: mandible 'criss-crossing' likely requires mandible pitch (rotation in the sagittal plane), in addition to yaw (rotation in the horizontal plane, figure 1*b*). We also observed this pitch movement in experiments with restrained live ants (figure 3*c*,*d*): when a worker ant was mounted such that her head was held steady and the left mandible was physically prevented from opening, the mandible moved downward upon interaction with the right mandible (figure 3*c*). When the right mandible re-opened, the left mandible sprang back to its initial position (figure 3*c* (iv)). This joint elasticity was retained in a freshly dissected ant head: when a gentle torque was applied to a closed mandible using tweezers, it pitched approximately about the horizontal axis of the vma, before returning to the original position upon removal of the torque (figure 3*d*(i–iv) and electronic supplementary material, video SV3)—a motion visually resembling the pitch observed in live ants (figure 2*d*(iv); electronic supplementary material, video SV4). Thus, the mandible joint articulation appears to permit pitch in regions of mandible overlap.

(c) Quantitative analysis of mandible kinematics

The 3D kinematic space occupied by mandible movements mirrored the qualitative observation of mandible movements during unrestrained cutting and biting: mandible motion is dominated by transverse adduction, but mandibles appeared to both pitch and yaw in regions of mandible overlap (see illustrative examples in figure 4*a*,*b* and electronic supplementary material, videos SV5 and SV6). In order to formally assess whether the overall motion patterns can be explained by rotation about a fixed axis, we subjected kinematic data from six *A. vollenweideri* specimens to quantitative kinematic analysis.

To test the hypothesis that ant mandibles rotate about a fixed point, we estimated the location of a joint centre as the coordinate that minimizes the variation in the distances between the joint centre estimate and mandible markers across the kinematic space (see equation (2.2)). A suitable way to assess the hypothesis is to inspect the variation of these distances: 1.62 ± 0.006, 1.07 ± 0.007 and 1.17 ± 0.008 mm for the distal, intermediate and proximal marker, respectively (between 90 and 185 distances for each of $n = 6$ ants, figure 4*c*). The standard deviation of these distance indicates negligible deviation from rotation about a fixed point: it corresponds to about three times the accuracy of the calibration target dimensions, about one image pixel, less than 1% of the mandible length, less than 5% of the effective in-lever, and is in good agreement with the standard deviation obtained from a physical hinge joint model, which serves as a proxy for experimental noise (3.526 ± 0.004, 2.361 ± 0.005, 2.311 ± 0.006 mm, respectively). Furthermore, the derived joint centre was in close proximity to the initial guess informed by morphology (putative joint centre): it was shifted toward

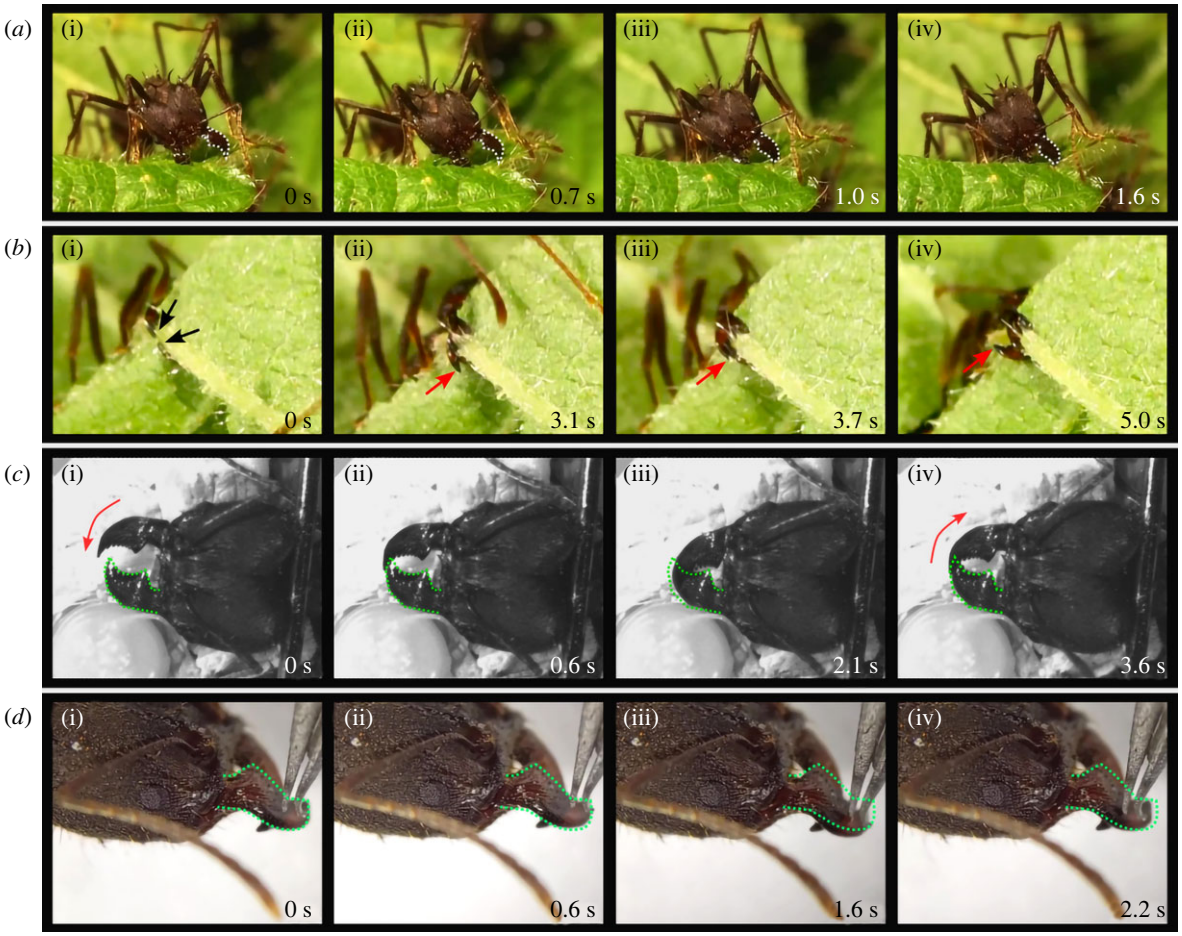

Figure 3. Qualitative observations of *Atta vollenweideri* mandible movement. (*a*(i–iv)) A worker ant uses her left mandible (dotted outline) to slice through bramble leaf lamina, which dominantly involves mandible yaw (transverse adduction, electronic supplementary material, video SV1). (*b*(i–iv)) A worker ant is cutting through a thick bramble leaf vein, viewed from below. The black arrows label the apical tooth of each mandible; the red arrows highlight the inferior mandible. In (*b*(ii) and (iii)), the right mandible is inferior, and in (*b*(iv)), the left mandible is inferior, indicating that mandible yaw was combined with pitch during these closing movements (electronic supplementary material, video SV2). (*c*(i–iv)) Mandible motion in a live but restrained worker. The left mandible (green outline) was physically prevented from opening, but the right mandible was free to move at will. From (*c*(i)–(iii)), the right mandible is superior. The position of the left mandible as seen in (*c*(i)) is imprinted in dotted green onto (*c*(i)–(iv)). In (*c*(iii)), the left mandible temporarily pitches downwards, and then returns to its previous position once the right mandible is no longer on top in (*c*(iv)), again illustrating that the mandible articulation permits mandible pitch when mandibles are fully closed. (*d*(i–iv)) A similar motion of the mandible can be reproduced through manual manipulation of a dissected worker ant head. Gentle application of a downward force with tweezers caused the right mandible (green outline) to pitch downwards (*d*(i–iii)). Upon removal of the force, the mandible rapidly returned to its initial position, as indicated again by the dashed green outline (*d*(iv)); also refer to electronic supplementary material, video SV3). Refer to figure 2 to infer approximate length-scales (all ants used were of similar size).

the sagittal plane by 0.067 ± 0.037 mm, or 5–10 pixels ($n = 6$, figure 4*f*). To test the hypothesis that ant mandibles rotate about a single axis with fixed orientation, we estimated the orientation of the axis that minimizes the variation of the angle spanned with two mandible-fixed line elements across the kinematic space—the bCAR (see equation (2.3)). For all but one ant, the residuals of at least one line element violated the assumptions of the regression analysis, indicating that a single axis cannot accurately explain the observed kinematics (see electronic supplementary material, figure S2 for detailed plots for all individuals; $n = 6$). Qualitative inspection of the residuals suggested that this result emerged from a systematic widening of the residuals in the region of mandible overlap, hinting at heteroscedasticity (figure 4*d*). In contrast, for widely open mandibles, the residuals were small and consistently close to the expected zero line (figure 4*d*,*e*). In order to account for this systematic pattern in our analysis, we next determined the largest movement range for which the residuals were uncorrelated, continuous, independent and normally distributed. To this end, we iteratively truncated the kinematic space to smaller and smaller movement ranges, starting from the region of mandible overlap where residuals appeared inflated. We then re-calculated the bCAR, residual angles, and the movement angle range after each truncation step, and re-tested the residual angles until all assumptions were met for both line elements (figure 4*d* and electronic supplementary material; Type 1 error rate was controlled via the Holm–Bonferroni method). This procedure suggested that mandible kinematics were consistent with rotation about a single fixed axis as long as opening angles were larger than $68 \pm 9°$; for reference, mandibles started to overlap for opening angles smaller than about 80°, and displayed a global minimum and maximum opening angle of 49 and 114° across all ants, respectively. The cut-off angle is thus consistent with the qualitative observations in freely cutting and biting ants, which suggested that mandibles can both pitch and yaw in the region of mandible overlap (figure 3*b* and electronic supplementary material, video SV2). The average cut-off angle was subsequently used to split the kinematics space of each individual into two characteristic regions. For

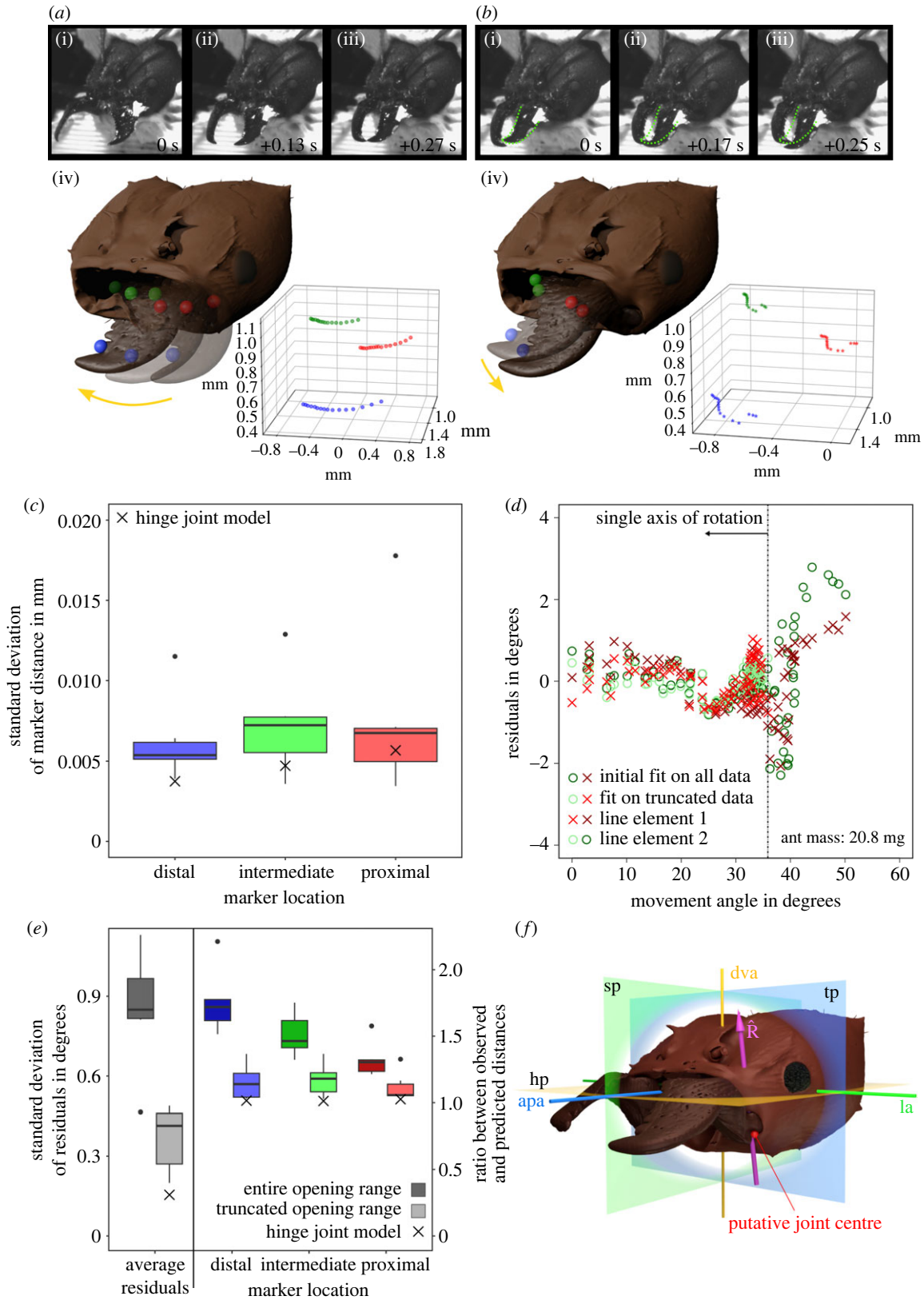

Figure 4. (*Caption overleaf.*)

each truncated region, the bCAR, the standard deviation of residuals and the distance metric were extracted separately, and compared with the global values across the entire kinematic space.

For opening angles greater than 68°, which encompass most of the mandible movement range, the inference that a single axis of rotation sufficiently explains the mandible kinematics was supported further by two independent pieces of evidence (figure 4*e*). First, both the standard deviation of the angle residuals and the distance metrics for all three markers decreased significantly ($0.85 \pm 0.22°$ versus $0.37 \pm 0.13°$; paired *t*-test: $t_5 = 7.17$, $p < 0.001$. Distal distance metric: 1.76 ± 0.24 versus 1.16 ± 0.13; paired *t*-test: $t_5 = 7.73$, $p < 0.001$; intermediate distance metric: 1.51 ± 0.16 versus 1.17 ± 0.12; paired *t*-test: $t_5 = 3.9$, $p < 0.05$; proximal distance metric: 1.32 ± 0.13 versus 1.12 ± 0.11; Wilcoxon rank sum test: $W = 21$, $p < 0.05$. $n = 6$ for all tests). To put both values into perspective, the corresponding results for the physical

Figure 4. (*Overleaf*.) Quantitative analysis of *Atta vollenweideri* mandible motion. Mandibles displayed one of two characteristic movement patterns, mirroring the qualitative observations reported in figure 3: (*a*) transverse adduction and abduction, i. e. mandible yaw; and (*b*) a combination of mandible yaw and pitch, which occurred exclusively in regions of mandible overlap. (*a*(i–iii)) Illustration of mandible yaw. (*a*(iv)) 3D rendering and 3D kinematics of mandible yaw (ant mass: 21.1 mg). (*b*(i–iii)) Illustration of mandible pitch and yaw. The initial position of the left mandible is highlighted in green. (*b*(iv)) 3D rendering and 3D kinematics of mandible pitch and yaw (ant mass: 21.1 mg). Coloured spheres represent the position of three tracked markers. (*c*) Quantitative kinematic analysis of data from six individuals confirmed that mandible movement is consistent with the expectation of rotation about a fixed point: the distances between markers and the estimated joint centre of rotation vary little across the kinematic space, and the average distance variation is comparable to the base line variation observed for a physical hinge joint model with comparable dimensions (crosses). (*d*) The variation of the angles formed by two line elements on the mandibles and the best continuous axis of rotation statistically violates the expectation for uniaxial rotation. Qualitative inspection of the data suggested that this violation arises from a widening of the residuals in the region of mandible overlap (large movement angles), reflecting heteroscedasticity (see electronic supplementary material, figure S2 for plots from all individuals). (*e*) To account for this observation, we estimated the largest movement angle range statistically consistent with uniaxial rotation. This analysis split the kinematic space into two characteristic regions (see main text for details): for small movement angles (large opening angles), mandible kinematics were consistent with the hinge joint hypothesis (truncated range; lighter shades on the plot). The standard deviation of residuals and the distance metrics were significantly reduced, and close to data obtained from a physical hinge joint model (crosses). In contrast, the statistical assumptions were violated for data from large movement angles (small opening angles; darker shades on the plot), indicating that rotation can be multi-axial in the region of mandible overlap (not shown). (*f*) The estimated dominant axis of rotation $\hat{\boldsymbol{R}}$ (pink) for large opening angles was closely aligned to the dorso-ventral head axis (dva), so lies approximately in the sagittal (sp) and transverse (tp) head planes, and is consequently about perpendicular to the lateral (la) and anterior–posterior (apa) head axes and horizontal head plane (hp). The location and orientation of $\hat{\boldsymbol{R}}$ was highly consistent across individuals, and close to the initial guess informed by morphology (red sphere).

hinge joint model were 0.16° and 1.02, 1.01 and 1.03 for the distal, intermediate and proximal distance metrics, respectively (figure 4*e*). Second, the orientation of the bCAR was highly consistent across individuals, with a mean deviation about the global average of $3.0 \pm 1.0°$ ($n = 6$, figure 4*f*). In all individuals, the rotational axis was approximately aligned with the dorso-ventral head axis (deviation of $6 \pm 2°$), and thus lies dominantly in the sagittal and transverse head planes (deviation of $4 \pm 2°$ for both, figure 4*f*). Given that the global orientation estimate is influenced by tracking error, fitting error, inaccuracy in head landmark placement, and biological variation, the small deviation across individuals strongly suggests a robust estimate of a consistently oriented bCAR in this region of the kinematic space.

By contrast, for opening angles smaller than 68°, the residuals of all but one ant still significantly violated the assumptions of the regression analysis for at least one line element (see electronic supplementary material, figure S3 for plots for all individuals; $n = 6$). Thus, rotation in this region is multi-axial, consistent with the initial speculation based on qualitative observations of mandible kinematics. In further support of this conclusion, both the standard deviation and the distance metrics in this region increased upon truncation ($1.05 \pm 0.26°$ for the standard deviation, and 2.59 ± 0.53; 1.88 ± 0.36 and 1.52 ± 0.22 for the distance metric of the distal, middle and proximal marker, respectively); the markers moved a distance of between 1.5 and 2.5 times the predicted values for rotation about one fixed axis.

4. Discussion

The majority of winged insects with biting–chewing mandibles are thought to exhibit obligate dicondyly: their mandible joints act as simple hinges, permitting only rotation about a single fixed axis. This supposed kinematic simplicity remains quantitatively unconfirmed, and stands in marked contrast to jaw movements in vertebrates, which often involve translation and multi-axial rotation. We used 3D motion capture and rigid body mechanics to conduct a direct test of the hinge joint hypothesis in *A. vollenweideri* leaf-cutter ants. Mandible kinematics were consistent with rotation about a single fixed axis across most of the kinematic space, but deviated from simple hinge joint kinematics around the region of mandible overlap. Hence, contrary to the long-held view that the dicondylic joints of winged biting–chewing insects are hinges, mandibles kinematics in leaf-cutter ants involve more than one DoF.

(a) The orientation of the dominant axis of rotation controls bite performance, and mandible yaw, roll and pitch

The majority of the kinematics space occupied by mandible movements reflected mandible yaw, and can be accurately described as rotation about a single dominant axis of rotation. This conclusion is supported by three independent lines of evidence. First, the distance between mandible markers and a derived joint centre is highly consistent across the kinematic space (figure 4*c*); second, fitting a single rotational axis to data from opening angles larger than 68° resulted in small and randomly distributed residuals of the cost function defined by equation (2.3) (figure 4*e*); and third, the standard deviation of the residuals and the distance metrics in this region of the kinematic space were small, and comparable to those obtained from a physical hinge joint model (figure 4*e*).

The orientation of the dominant axis defines the plane of rotation, and thus determines the magnitude of the mechanical advantage of the force transmission system [25,33,35,41], the possible mandibular gape with respect to the head- or body-fixed anatomical planes [25,33,41], and the angle between apodeme and effective in-lever [41]. All these parameters play a crucial role in determining insect bite performance [41]. All previous work in insects implicitly or explicitly assumed that the mandible rotational axis has a fixed orientation and location, so that a unique instantaneous mechanical advantage can be defined [25,33,35,40,41,86,88,89]. Our results in *A. vollenweideri* indeed suggest that the rotational axis has an approximately fixed position, but for two reasons, this should only be a minor source of comfort for those interested in exact mechanical models of insect bite performance. First, joint articulations in insects are distinct from idealized shapes such as spheres or cylinders, and there is no strong reason to postulate *a priori* that the location of the rotational axis is generally fixed in space. Vertebrate joints virtually never have an instantaneous rotational axis that is fixed in space, and there is little reason to assume this is consistently

different in insects. Second, even seemingly negligible movements of the joint centre can cause significant errors in mechanical calculations. As an illustrative example, a 2 cm misplacement of the human hip joint centre results in a decrease of the transmittable muscle moment of close to 50% [90]. The key problem is that insect skeletal segments are small, so that highly accurate 3D data are required to resolve relevant displacements. It is conceivable that variation of the mechanical advantage due to small movements of the joint centre explains some of the residual variation in *Atta* bite force that cannot be captured by mechanical models that assume a fixed joint centre location [41].

The functional implications of the rotational axis for bite mechanics are well appreciated, but the behavioural and functional significance of its orientation with respect to a head- or mandible-fixed coordinate system has received less attention [25,50–52]. In early hexapods, $\hat{\boldsymbol{R}}$ appears to be closely aligned with the distal incisivi and is nearly orthogonal to 'molar areas' [25]. Mandibles dominantly rotate about their long axis, and this rolling motion may aid grinding, but limits the possible mandible gape [25]. In silverfish (Zygentoma) and winged insects (Pterygota), $\hat{\boldsymbol{R}}$ shifted; it is oriented more towards the cephalo-caudal head axis in orthognathous and hypognathous insects [25], or the dorso-ventral head axis in prognathous insects. Consistent with this general trend, the dominant rotational axis in prognathous *A. vollenweideri* deviates by less than 6° from the dorso-ventral axis. Mandible rotation thus largely involves yaw, i.e. contraction of the mandible opener and closer muscles results in transverse mandible abduction and adduction, respectively. By contrast to the roll of early hexapod mandibles, mandible yaw enables large mandible gapes [25], which are essential for ants that use their mandibles to grasp objects comparable in size to their head width, such as brood, or, more specific to the leaf-cutters, to cut large fragments from leaf laminas (figure 4*a*(i–iv) and electronic supplementary material, video SV3). However, alternative orientations may bring other functional benefits. In general, if the rotational axis has components in more than one of the three body planes, the mandible opening angle will have components in all three planes—mandibles will yaw, roll and pitch with respect to head-fixed reference planes. Thus, bi-axial mandible movement with respect to head or body planes, as observed in a trap-jaw and a ponerine ant [49,50], is not conclusive evidence against hinge joint kinematics *per se*. Instead, it may merely suggest an inclined rotational axis, advantageous because it may allow ants to handle objects of different sizes with different parts of their mandibles [50–52].

(b) The origin and functional significance of mandible pitch

Qualitative observations of mandible movements during cutting and biting suggested that mandibles can pitch: both the left and right mandibles can be superior when mandibles are closed, and swaps in position occurred across repeated closing cycles (figures 3 and 4 and electronic supplementary material, videos SV4 and SV7). Quantitative evidence for pitch was extracted from 3D kinematics data: for opening angles smaller than 68°, the residual angles unexplained by the bCAR varied systematically with the movement angle (see electronic supplementary material, figure S3), and the mandible markers moved distances considerably larger than expected from rotation about a fixed axis (figure 4*e*). Thus, our results provide strong evidence against the null hypothesis of a simple hinge joint in *A. vollenweideri* ants. How is mandible pitch actuated, and what is its biological function?

Each mandible in *A. vollenweideri* is actuated by a single pair of antagonistic muscles. Each muscle is attached to the mandible via its own apodeme, and thus has one main line of action [86]. Activation of these muscles results in rotation or translation of the mandible, unless the net muscle force and moment are balanced by reaction forces and moments sustained by the joint articulation (or by the reactions associated with bites into a stiff object). Because the reaction sustainable by the joint depends on the joint articulation, and because the shape of this articulation may vary with opening angle (see e.g. [53,55]), it is conceivable that the sustainable reactions vary as the mandible rotates, so permitting multi-axial orientation in restricted sections of the kinematic space. Thus, even a simple antagonistic muscle pair can in principle drive complex rotation and translation. In *Atta*, the net muscle vector is almost perfectly aligned with the anterior–posterior axis [41,86], and can thus induce both yaw and pitch moments. Perhaps pitch is blocked by the articulations at large mandible gape, but becomes possible in the region of mandible overlap, as indicated by the presence of a gap between the dma and the head-capsule for the inferior mandible (figure 2). Alternatively, multi-axial kinematics may result from the interaction of the two mandibles: the reaction at the contact point between both mandibles could induce pitch, in addition to muscle-driven yaw. Indeed, we did not observe deviations from rotation about the bCAR when mandibles were far away from each other, which is consistent with, if not sufficient to conclusively support, both hypotheses. Pitch of overlapping mandibles was also recently observed in *Odontomachus brunneus* trap-jaw ants: during rapid mandible closure, mandibles first followed a circular trajectory, but out-of-plane movements occurred as mandibles overlapped [91]. Re-direction of muscle forces via reaction forces between mandibles, or a variation of sustainable joint reactions due the changes in articulation shape, may be two valuable strategies to enable more complex 'mastication-like' kinematics of dicondylic mandibles, without the need to resort to more complicated and energetically costly direct actuation via different muscle groups.

Based on our observations of both unrestrained and restrained cutting, we suggest three functional benefits of mandible pitch. First, leaf-cutter ants frequently use their mandibles like scissors, for example when they initiate cuts at the free edge of a leaf lamina [92,93]. As any hairdresser can attest, scissors need to be tight to function, and in man-made scissors, this is typically ensured by a screw that connects two blades, each with a slight inward curvature, at a shared pivot point. As the scissors are drawn close, the blades bend, and the stored elastic strain energy helps to keep the gap between the blades small, and the scissors tight [94]. In *A. vollenweideri*, a similar effect may help to keep the blades tightly connected during scissor-cutting. Indeed, in both living and dead specimens of *A. vollenweideri*, the gap between the two mandibles was narrow (figures 2*a*(i) and 4*b*), and mandibles of dead ants sprang back to their original position after pitch was induced by application of an external torque, indicating joint elasticity. Second, during the cutting of tough materials such as primary or

secondary leaf veins [95], mandible criss-crossing may help to find a path of least resistance, and thus reduce the mechanical effort for cutting. Indeed, mandible criss-crossing and slight re-orientations of the mandibles were often observed when ants made repeated attempts to cut through thick leaf veins (figure 3*b* and supplementary material in [92]), reminiscent of how we may attempt to cut a thick wire with pliers or a thick tree branch with loppers. Third, mandible pitch may prevent damage to the sharp cutting edge during mandible impact. In one behavioural observation, a worker ant was cutting through a thin polymer sheet, which bent easily and unpredictably (electronic supplementary material, video SV7). When the ant attempted to close its mandibles, the sheet flexed and the left mandible went rapidly from superior to inferior and back.

(c) Mandible kinematics and joint morphology in Dicondylia are more diverse than traditionally assumed

We have demonstrated that *A. vollenweideri* mandible joints have more than one DoF. Mandible joints with multiple DoFs were likely the original condition in early hexapods, which possessed monocondylic mandibles actuated by multiple muscle groups [25]. Silverfish and firebrats (Zygentoma), jumping bristletails (Archaeognatha) and mayflies (Ephemeroptera) have retained a complex muscular actuation, but mandible motion appears to be more tightly constrained by a set of non-permanent articulations [22,24,25], which may allow 'gliding movements' in addition to rotation [20,22]. These taxa thus share a more complex mandible muscle actuation with early monocondylic hexapods, but possess more restrictive mandible joint articulations reminiscent of obligate dicondyly—a trait combination that has consequently been referred to as 'facultative dicondyly' [22]. In Odonata and Neoptera with biting mouthparts, muscle actuation reduced to a single pair of antagonistic muscles, and the consensus is that two conspicuous condyles restrict mandible kinematics to rotation about a single axis; mandibles are obligately dicondylic [25]. Remarkably, a reversion to a more complex muscle actuation and less restrictive joint articulations appears to have occurred in a group of parasitic wasps (Chalcidoidea), which was reported to have a strongly reduced posterior condyle and a modified musculature [31]. These modifications presumably enable active actuation of multiple DoFs [31]. In light of its resemblance to the ancestral trait of early hexapods, this mandible joint configuration has been referred to as 'secondary monocondyly' [31]. In *A. vollenweideri*, joint articulations also depart from classic dicondyly: the ventral articulation (vma) resembles a ball-and-socket joint, but the dorsal articulation (dma) is elongated, cylindrical, and thus conspicuously distinct from the vma in shape (figure 2*a*). Without the coupling of dorsal and ventral ball-and-socket joints to constrain the mandible—as observed in obligate dicondylic taxa—additional DoFs become accessible. On the basis of these observations, it is evident that neither facultative dicondyly, obligate dicondyly, nor secondary monocondyly adequately describes the mandibles of *A. vollenweideri*. Instead, we propose that they represent 'secondary facultative dicondyly,' characterized by the following conditions: (i) two condyles exist, but have distinct morphology; (ii) mandible kinematics involve more than one DoF, but the dominant movement is rotation about a single fixed axis, actuated by a single antagonistic pair of muscles; and (iii) additional DoFs emerge through changes in sustainable joint reaction throughout the kinematic space, or via physical interactions between overlapping mandibles. Recently, an elongated dma has been identified as a characteristic trait of the Formicidae [54,96], raising the possibility that secondary facultative dicondyly may be widespread in ants.

Jaw kinematics in vertebrates have received significant attention, but the equivalent problem in insects remains quantitatively unexplored. There is an increasing body of evidence that suggests that insect mandible kinematics are considerably more diverse than traditionally appreciated—representatives of at least two insect families that were thought to have simple hinge joints are capable of more complex mandible movements. Why did some neopteran taxa shift away from obligate dicondyly? Perhaps the more diverse mandible movement repertoire of wingless hexapods confers functional advantages that remain under-appreciated [25]. Quantitative comparative studies are necessary to unravel the evolutionary pathways and driving factors that lead to a reversion to more complex mandible movements in some insects, and to understand their functional consequences.

Ethics. This work did not require ethical approval from a human subject or animal welfare committee.

Data accessibility. Raw data used for final analyses in the form of CSV files have been included as electronic supplementary material [97].

Declaration of AI use. We have not used AI-assisted technologies in creating this article.

Authors' contributions. V.K.: conceptualization, data curation, formal analysis, investigation, methodology, project administration, visualization, writing—original draft, writing—review and editing; F.P.: conceptualization, formal analysis, investigation, methodology, project administration, writing—original draft, writing—review and editing; D.L.: conceptualization, formal analysis, funding acquisition, methodology, project administration, supervision, validation, writing—original draft, writing—review and editing.

All authors gave final approval for publication and agreed to be held accountable for the work performed herein.

Conflict of interest declaration. We declare we have no competing interests.

Funding. This study is part of a project that has received funding from the European Research Council (ERC) under the European Union's Horizon 2020 Research and Innovation Programme (grant agreement no. 851705) and a Human Frontier Science Programme Young Investigator Award (grant no. RGY0073/2020), both to D.L.

Acknowledgements. We thank Professor Flavio Roces for his generous support, and for gifting the *Atta vollenweideri* colony used in this work, Professor Tyson Hedrick for rapid replies and valuable advice on using DLTdv8a, and Professor Alexander Blanke for stimulating discussions on insect mandible joints. We also thank the Company of Biologists and the Society for Experimental Biology (SEB) for funding the Open Biomechanics sessionat SEB 2022 annual conference that brought the contributors together for this theme issue.

References

1. Deakin WJ, Anderson PSL, Smith TJ, Hill JJ, Rücklin M, Donoghue PCJ, Rayfield EJ. 2023 Increasing morphological disparity and decreasing optimality for jaw speed and strength during the radiation of jawed vertebrates. *Sci. Adv.* **8**, eabl3644. (doi:10.1126/sciadv.abl3644)

2. Olsen AM, Hernandez LP, Brainerd EL. 2020 Multiple degrees of freedom in the fish skull and their relation to hydraulic transport of prey in channel catfish. *Integr. Org. Biol.* **2**, obaa031. (doi:10.1093/iob/obaa031)
3. Hiiemae KM. 1978 Mammalian mastication: a review of the activity of the jaw muscles and the movements they produce in chewing. *Dev. Funct. Evol. Teeth* **1978**, 359–398.
4. Herring SW. 1993 Functional morphology of mammalian mastication. *Am. Zool.* **33**, 289–299. (doi:10.1093/icb/33.3.289)
5. Koolstra J. 2002 Dynamics of the human masticatory system. *Crit. Rev. Oral. Biol. Med.* **13**, 366–376. (doi:10.1177/154411130201300406)
6. Iriarte-Díaz J, Reed DA, Ross CF. 2011 Sources of variance in temporal and spatial aspects of jaw kinematics in two species of primates feeding on foods of different properties. *Integr. Comp. Biol.* **51**, 307–319. (doi:10.1093/icb/icr072)
7. Terhune CE, Iriarte-Díaz J, Taylor AB, Ross CF. 2011 The instantaneous center of rotation of the mandible in nonhuman primates. *Integr. Comp. Biol.* **51**, 320–332. (doi:10.1093/icb/icr031)
8. Menegaz RA, Baier DB, Metzger KA, Herring SW, Brainerd EL. 2015 XROMM analysis of tooth occlusion and temporomandibular joint kinematics during feeding in juvenile miniature pigs. *J. Exp. Biol.* **218**, 2573–2584. (doi:10.1242/jeb.119438)
9. Bhullar BAS, Manafzadeh AR, Miyamae JA, Hoffman EA, Brainerd EL, Musinsky C, Crompton AW. 2019 Rolling of the jaw is essential for mammalian chewing and tribosphenic molar function. *Nature* **566**, 528–532. (doi:10.1038/s41586-019-0940-x)
10. Gidmark NJ, Tarrant JC, Brainerd EL. 2014 Convergence in morphology and masticatory function between the pharyngeal jaws of grass carp, *Ctenopharyngodon idella*, and oral jaws of amniote herbivores. *J. Exp. Biol.* **217**, 1925–1932. (doi:10.1242/jeb.096248)
11. Kolmann MA, Welch KC, Summers AP, Lovejoy NR. 2016 Always chew your food: freshwater stingrays use mastication to process tough insect prey. *Proc. R. Soc. B* **283**, 20161392. (doi:10.1098/rspb.2016.1392)
12. Laurence-Chasen JD, Ramsay JB, Brainerd EL. 2019 Shearing overbite and asymmetrical jaw motions facilitate food breakdown in a freshwater stingray, *Potamotrygon motoro*. *J. Exp. Biol.* **222**, jeb197681. (doi:10.1242/jeb.197681)
13. Schwarz D, Konow N, Roba YT, Heiss E. 2020 A salamander that chews using complex, three-dimensional mandible movements. *J. Exp. Biol.* **223**, jeb220749. (doi:10.1242/jeb.220749)
14. Keefe DF, O'Brien TM, Baier DB, Gatesy SM, Brainerd EL, Laidlaw DH. 2008 Exploratory visualization of animal kinematics using instantaneous helical axes. *Comput. Graph. Forum* **27**, 863–870. (doi:10.1111/j.1467-8659.2008.01218.x)
15. Brainerd EL, Baier DB, Gatesy SM, Hedrick TL, Metzger KA, Gilbert SL, Crisco JJ. 2010 X-ray reconstruction of moving morphology (XROMM): precision, accuracy and applications in comparative biomechanics research. *J. Exp. Zool. Suppl. A Ecol. Genet. Physiol.* **313A**, 262–279. (doi:10.1002/jez.589)
16. Montuelle SJ, Olson RA, Curtis H, Beery S, Williams SH. 2020 Effects of food properties on chewing in pigs: flexibility and stereotypy of jaw movements in a mammalian omnivore. *PLoS ONE* **15**, e0228619. (doi:10.1371/journal.pone.0228619)
17. Brainerd EL, Camp AL. 2019 Functional morphology of vertebrate feeding systems: new insights from XROMM and fluoromicrometry. In *Feeding in vertebrates: evolution, morphology, behavior, biomechanics* (eds V Bels, IQ Whishaw), pp. 21–44. Cham, Switzerland: Springer International Publishing.
18. Schmitt C, Rack A, Betz O. 2014 Analyses of the mouthpart kinematics in *Periplaneta americana* (Blattodea, Blattidae) using synchrotron-based X-ray cineradiography. *J. Exp. Biol.* **217**, 3095–3107. (doi:10.1242/jeb.092742)
19. Josten B, Gorb SN, Büsse S. 2022 The mouthparts of the adult dragonfly *Anax imperator* (Insecta: Odonata), functional morphology and feeding kinematics. *J. Morphol.* **283**, 1163–1181. (doi:10.1002/jmor.21497)
20. Krenn HW. 2019 *Insect mouthparts: form, function, development and performance*. Cham, Switzerland: Springer Nature.
21. Krenn HW. 2019 Form and function of insect mouthparts. In *Insect mouthparts. Form, function, development and performance* (ed. HW Krenn), pp. 9–46. Berlin, Germany: Springer.
22. Staniczek AH. 2000 The mandible of silverfish (Insecta: Zygentoma) and mayflies (Ephemeroptera): its morphology and phylogenetic significance. *Zool. Anz.* **239**, 147–178.
23. Koch M. 2001 Mandibular mechanisms and the evolution of hexapods. *Ann. Soc. Entomol. Fr.* **37**, 129–174.
24. Blanke A, Machida R, Szucsich NU, Wilde F, Misof B. 2015 Mandibles with two joints evolved much earlier in the history of insects: dicondyly is a synapomorphy of bristletails, silverfish and winged insects. *Syst. Entomol.* **40**, 357–364. (doi:10.1111/syen.12107)
25. Blanke A. 2019 The early evolution of biting-chewing performance in Hexapoda. In *Insect mouthparts. Form, function, development and performance* (ed. HW Krenn), pp. 175–202. Berlin, Germany: Springer.
26. Blanke A, Watson PJ, Holbrey R, Fagan MJ. 2017 Computational biomechanics changes our view on insect head evolution. *Proc. R. Soc. B* **284**, 20162412. (doi:10.1098/rspb.2016.2412)
27. Snodgrass R. 1935 *Principles of insect morphology*. New York, NY: McGraw-Hill Book Company.
28. Wipfler B, Machida R, Mueller B, Beutel RG. 2011 On the head morphology of Grylloblattodea (Insecta) and the systematic position of the order, with a new nomenclature for the head muscles of Dicondylia. *Syst. Entomol.* **36**, 241–266. (doi:10.1111/j.1365-3113.2010.00556.x)
29. Blanke A, Wipfler B, Letsch H, Koch M, Beckmann F, Beutel R, Misof B. 2012 Revival of Palaeoptera—head characters support a monophyletic origin of Odonata and Ephemeroptera (Insecta). *Cladistics* **28**, 560–581. (doi:10.1111/j.1096-0031.2012.00405.x)
30. Beutel RG, Friedrich F, Yang XK, Ge SQ. 2013 *Insect morphology and phylogeny: a textbook for students of entomology*. Berlin, Germany: De Gruyter.
31. van de Kamp T *et al.* 2022 Evolution of flexible biting in hyperdiverse parasitoid wasps. *Proc. R. Soc. B* **289**, 20212086. (doi:10.1098/rspb.2021.2086)
32. David S, Funken J, Potthast W, Blanke A. 2016 Musculoskeletal modelling of the dragonfly mandible system as an aid to understanding the role of single muscles in an evolutionary context. *J. Exp. Biol.* **219**, 1041–1049. (doi:10.1242/jeb.132399)
33. Weihmann T, Reinhardt L, Weißing K, Siebert T, Wipfler B. 2015 Fast and powerful: biomechanics and bite forces of the mandibles in the American cockroach *Periplaneta americana*. *PLoS ONE* **10**, e0141226. (doi:10.1371/journal.pone.0141226)
34. Li D, Zhang K, Zhu P, Wu Z, Zhou H. 2011 3D configuration of mandibles and controlling muscles in rove beetles based on micro-CT technique. *Anal. Bioanal. Chem.* **401**, 817–825. (doi:10.1007/s00216-011-5088-y)
35. Goyens J, Dirckx J, Dierick M, Van Hoorebeke L, Aerts P. 2014 Biomechanical determinants of bite force dimorphism in *Cyclommatus metallifer* stag beetles. *J. Exp. Biol.* **217**, 1065–1071. (doi:10.1242/jeb.091744)
36. Bitsch J. 1994 The morphological groundplan of Hexapoda: critical review of recent concepts. *Ann. Soc. Entomol. Fr. (New Series)* **30**, 103–129. (doi:10.1080/21686351.1994.12278837)
37. Fürst von Lieven A. 2000 The transformation from monocondylous to dicondylous mandibles in the insecta. *Zool. Anz.* **239**, 139–146.
38. Gayubo SF. 2008 Mouthparts of hexapods. In *Encyclopedia of entomology* (ed. JL Capinera), pp. 2497–2504. Berlin, Germany: Springer.
39. Gronenberg W. 1995 The fast mandible strike in the trap-jaw ant *Odontomachus*—I. Temporal properties and morphological characteristics. *J. Comp. Physiol. A* **176**, 391–398. (doi:10.1007/BF00219064)
40. David S, Funken J, Potthast W, Blanke A. 2016 Musculoskeletal modelling under an evolutionary perspective: deciphering the role of single muscle regions in closely related insects. *J. R. Soc. Interface* **13**, 20160675. (doi:10.1098/rsif.2016.0675)
41. Püffel F, Johnston R, Labonte D. 2023 A biomechanical model for the relation between bite force and mandibular opening angle in arthropods. *R. Soc. Open Sci.* **10**, 221066. (doi:10.1098/rsos.221066)
42. Ross CF, Iriarte-Diaz J. 2019 Evolution, constraint, and optimality in primate feeding systems. In *Feeding in vertebrates: evolution, morphology, behavior, biomechanics* (eds V Bels, IQ Whishaw), pp. 787–829. Cham, Switzerland: Springer International Publishing.
43. Martin T, von Koenigswald W (eds). 2020 *Mammalian teeth: form and function*. Munich, Germany: Verlag Dr. Friederich Pfiel.

44. Isely FB. 1944 Correlation between mandibular morphology and food specificity in grasshoppers. *Ann. Entomol. Soc. Am.* **37**, 47–67. (doi:10.1093/aesa/37.1.47)
45. Chapman R. 1964 The structure and wear of the mandibles in some African grasshoppers. *Proc. Zool. Soc. Lond.* **142**, 107–122. (doi:10.1111/j.1469-7998.1964.tb05157.x)
46. Bernays EA. 1991 Evolution of insect morphology in relation to plants. *Phil. Trans. R. Soc. Lond. B* **333**, 257–264. (doi:10.1098/rstb.1991.0075)
47. Chapman R. 1995 Mechanics of food handling by chewing insects. In *Regulatory mechanisms in insect feeding* (eds RF Chapman, G de Boer), pp. 3–31. Berlin, Germany: Springer.
48. Clissold F. 2007 The biomechanics of chewing and plant fracture: mechanisms and implications. *Adv. Insect Physiol.* **34**, 317–372. (doi:10.1016/S0065-2806(07)34006-X)
49. Gronenberg W, Brandão CRF, Dietz BH, Just S. 1998 Trap-jaws revisited: the mandible mechanism of the ant *Acanthognathus*. *Physiol. Entomol.* **23**, 227–240. (doi:10.1046/j.1365-3032.1998.233081.x)
50. Zhang W, Li M, Zheng G, Guan Z, Wu J, Wu Z. 2020 Multifunctional mandibles of ants: variation in gripping behavior facilitated by specific microstructures and kinematics. *J. Insect Physiol.* **120**, 103993. (doi:10.1016/j.jinsphys.2019.103993)
51. Zhang W, He Z, Sun Y, Wu J, Wu Z. 2020 A mathematical modeling method elucidating the integrated gripping performance of ant mandibles and bio-inspired grippers. *J. Bionic Eng.* **17**, 732–746. (doi:10.1007/s42235-020-0065-9)
52. Zhang W, Wu Z, Wang Z, Wang Z, Li C, Rajabi H, Wu J. 2021 Double-rowed teeth: design specialization of the *H. venator* ants for enhanced tribological stability. *Bioinspir. Biomim.* **16**, 055003. (doi:10.1088/1748-3190/ac124a)
53. Richter A, Garcia FH, Keller RA, Billen J, Katzke J, Boudinot BE, Economo EP, Beutel RG. 2021 The head anatomy of *Protanilla lini* (Hymenoptera: Formicidae: Leptanillinae), with a hypothesis of their mandibular movement. *Myrmecol. News* **31**, 85–114. (doi:10.25849/myrmecol.news_031:085)
54. Boudinot BE, Khouri Z, Richter A, Griebenow ZH, Barden P. 2022 Evolution and systematics of the Aculeata and kin (Hymenoptera), with emphasis on the ants (Formicoidea: †@@@idae fam. nov., Formicidae). *BioRxiv*, 2022.02.20.480183. (doi:10.1101/2022.02.20.480183)
55. Richter A, Boudinot BE, Garcia FH, Billen J, Economo EP, Beutel RG. 2023 Wonderfully weird: the head anatomy of the armadillo ant, *Tatuidris tatusia* (Hymenoptera: Formicidae: Agroecomyrmecinae), with evolutionary implications. *Myrmecol. News* **33**, 35–75. (doi:10.25849/myrmecol.news_033:035)
56. Keller RA. 2011 A phylogenetic analysis of ant morphology (Hymenoptera: Formicidae) with special reference to the poneromorph subfamilies. *Bull. Am. Mus. Nat. Hist.* **2011**, 355. (doi:10.1206/355.1)
57. Vagts S, Schlattmann J, Busshardt P, Kleinteich T, Gorb SN. 2017 The application of multi-body simulation approach in the kinematic analysis of beetle leg joints. *Artif. Life Robot.* **22**, 412–420. (doi:10.1007/s10015-017-0386-x)
58. Weber NA. 1972 The fungus-culturing behaviour of ants. *Am. Zool.* **12**, 577–587. (doi:10.1093/icb/12.3.577)
59. Wilson EO. 1980 Caste and division of labor in leaf-cutter ants (Hymenoptera: Formicidae: *Atta*): I. The overall pattern in *A. sextens*. *Behav. Ecol. Sociobiol.* **7**, 143–156. (doi:10.1007/BF00299520)
60. Wirth R, Herz H, Ryel RJ, Beyschlag W, Hölldobler B. 2003 *Herbivory of leaf-cutting ants: a case study on Atta colombica in the tropical rainforest of panama*. Berlin, Germany: Springer Science & Business Media.
61. Swanson AC *et al.* 2019 Welcome to the *Atta* world: a framework for understanding the effects of leaf-cutter ants on ecosystem functions. *Funct. Ecol.* **33**, 1386–1399. (doi:10.1111/1365-2435.13319)
62. Weihmann T, Karner M, Full RJ, Blickhan R. 2010 Jumping kinematics in the wandering spider *Cupiennius salei*. *J. Comp. Physiol. A Neuroethol. Sens. Neural Behav. Physiol.* **196**, 421–438. (doi:10.1007/s00359-010-0527-3)
63. Knorlein BJ, Baier DB, Gatesy SM, Laurence-Chasen JD, Brainerd EL. 2016 Validation of XMALab software for marker-based XROMM. *J. Exp. Biol.* **219**, 3701–3711. (doi:10.1242/jeb.145383)
64. Hedrick TL. 2008 Software techniques for two- and three-dimensional kinematic measurements of biological and biomimetic systems. *Bioinspir. Biomim.* **3**, 034001. (doi:10.1088/1748-3182/3/3/034001)
65. Theriault DH, Fuller NW, Jackson BE, Bluhm E, Evangelista D, Wu Z, Betke M, Hedrick TL. 2014 A protocol and calibration method for accurate multi-camera field videography. *J. Exp. Biol.* **217**, 1843–1848. (doi:10.1242/jeb.100529)
66. Schindelin J *et al.* 2012 Fiji: an open-source platform for biological-image analysis. *Nat. Methods* **9**, 676–682. (doi:10.1038/nmeth.2019)
67. Richter A, Garcia FH, Keller RA, Billen J, Economo EP, Beutel RG. 2020 Comparative analysis of worker head anatomy of *Formica* and *Brachyponera* (Hymenoptera: Formicidae). *Arthropod Syst. Phyl.* **78**, 133–170. (doi:10.26049/ASP78-1-2020-06)
68. Youm Y, Yoon YS. 1979 Analytical development in investigation of wrist kinematics. *J. Biomech.* **12**, 613–621. (doi:10.1016/0021-9290(79)90082-4)
69. Stokdijk M, Meskers C, Veeger H, De Boer Y, Rozing P. 1999 Determination of the optimal elbow axis for evaluation of placement of prostheses. *Clin. Biomech.* **14**, 177–184. (doi:10.1016/S0268-0033(98)00057-6)
70. Cerveri P, Lopomo N, Pedotti A, Ferrigno G. 2005 Derivation of centers and axes of rotation for wrist and fingers in a hand kinematic model: methods and reliability results. *Ann. Biomed. Eng.* **33**, 402–412. (doi:10.1007/s10439-005-1743-9)
71. Chang LY, Pollard NS. 2007 Robust estimation of dominant axis of rotation. *J. Biomech.* **40**, 2707–2715. (doi:10.1016/j.jbiomech.2007.01.010)
72. Chin A, Lloyd D, Alderson J, Elliott B, Mills P. 2010 A marker-based mean finite helical axis model to determine elbow rotation axes and kinematics *in vivo*. *J. Appl. Biomech.* **26**, 305–315. (doi:10.1123/jab.26.3.305)
73. Soutas-Little RW, Inman DJ, Balint D. 2008 *Engineering mechanics: dynamics – computational edition*. Henderson, KY: Thompson International.
74. Spoor C, Veldpaus F. 1980 Rigid body motion calculated from spatial co-ordinates of markers. *J. Biomech.* **13**, 391–393. (doi:10.1016/0021-9290(80)90020-2)
75. Woltring HJ, Huiskes R, De Lange A, Veldpaus FE. 1985 Finite centroid and helical axis estimation from noisy landmark measurements in the study of human joint kinematics. *J. Biomech.* **18**, 379–389. (doi:10.1016/0021-9290(85)90293-3)
76. Woltring HJ. 1991 Representation and calculation of 3-D joint movement. *Hum. Mov. Sci.* **10**, 603–616. (doi:10.1016/0167-9457(91)90048-3)
77. Halvorsen K, Lesser M, Lundberg A. 1999 A new method for estimating the axis of rotation and the center of rotation. *J. Biomech.* **32**, 1221–1227. (doi:10.1016/S0021-9290(99)00120-7)
78. Fraysse F, Thewlis D. 2014 Comparison of anatomical, functional and regression methods for estimating the rotation axes of the forearm. *J. Biomech.* **47**, 3488–3493. (doi:10.1016/j.jbiomech.2014.09.003)
79. Ehrig RM, Heller MO. 2019 On intrinsic equivalences of the finite helical axis, the instantaneous helical axis, and the SARA approach. A mathematical perspective. *J. Biomech.* **84**, 4–10. (doi:10.1016/j.jbiomech.2018.12.034)
80. Ancillao A, Vochten M, Verduyn A, De Schutter J, Aertbeliën E. 2022 An optimal method for calculating an average screw axis for a joint, with improved sensitivity to noise and providing an analysis of the dispersion of the instantaneous axes. *PLoS ONE* **17**, e0275218. (doi:10.1371/journal.pone.0275218)
81. Gamage SSHU, Lasenby J. 2002 New least squares solutions for estimating the average centre of rotation and the axis of rotation. *J. Biomech.* **35**, 87–93. (doi:10.1016/S0021-9290(01)00160-9)
82. Schwartz MH, Rozumalski A. 2005 A new method for estimating joint parameters from motion data. *J. Biomech.* **38**, 107–116. (doi:10.1016/j.jbiomech.2004.03.009)
83. Ehrig RM, Taylor WR, Duda GN, Heller MO. 2007 A survey of formal methods for determining functional joint axes. *J. Biomech.* **40**, 2150–2157. (doi:10.1016/j.jbiomech.2006.10.026)
84. Rodrigues O. 1840 Des lois géométriques qui régissent les déplacements d'un système solide dans l'espace, et de la variation des coordonnées provenant de ces déplacements considérés indépendamment des causes qui peuvent les produire. *J. Math. Pure Appl.* **5**, 380–440. [In French.]
85. Peña EA, Slate EH. 2006 Global validation of linear model assumptions. *J. Am. Stat. Assoc.* **101**, 341–354. (doi:10.1198/016214505000000637)
86. Püffel F, Pouget A, Liu X, Zuber M, van de Kamp T, Roces F, Labonte D. 2021 Morphological determinants of bite force capacity in insects: a biomechanical analysis of polymorphic leaf-cutter ants. *J. R. Soc. Interface* **18**, 20210424.

87. Cignoni P, Callieri M, Corsini M, Dellepiane M, Ganovelli F, Ranzuglia G. 2008 Meshlab: an open-source mesh processing tool. In *Eurographics Italian chapter conference*, vol. 2008, pp. 129–136. Italy: Salerno.
88. Blanke A, Schmitz H, Patera A, Dutel H, Fagan MJ. 2017 Form-function relationships in dragonfly mandibles under an evolutionary perspective. *J. R. Soc. Interface* **14**, 20161038. (doi:10.1098/rsif.2016.1038)
89. Püffel F, Roces F, Labonte D. 2023 Strong positive allometry of bite force in leaf-cutter ants increases the range of cuttable plant tissues. *bioRxiv*, p. 2022.09.28.509980.
90. Delp SL, Maloney W. 1993 Effects of hip center location on the moment-generating capacity of the muscles. *J. Biomech.* **26**, 485–499. (doi:10.1016/0021-9290(93)90011-3)
91. Sutton GP, St Pierre R, Kuo CY, Summers AP, Bergbreiter S, Cox S, Patek SN. 2022 Dual spring force couples yield multifunctionality and ultrafast, precision rotation in tiny biomechanical systems. *J. Exp. Biol.* **225**, jeb244077. (doi:10.1242/jeb.244077)
92. Schofield RM, Emmett KD, Niedbala JC, Nesson M. 2011 Leaf-cutter ants with worn mandibles cut half as fast, spend twice the energy, and tend to carry instead of cut. *Behav. Ecol. Sociobiol.* **65**, 969–982. (doi:10.1007/s00265-010-1098-6)
93. Schofield RM, Choi S, Coon JJ, Goggans MS, Kreisman TF, Silver DM, Nesson MH. 2016 Is fracture a bigger problem for smaller animals? Force and fracture scaling for a simple model of cutting, puncture and crushing. *Interface Focus* **6**, 20160002. (doi:10.1098/rsfs.2016.0002)
94. Sanson G, Read J, Aranwela N, Clissold F, Peeters P. 2001 Measurement of leaf biomechanical properties in studies of herbivory: opportunities, problems and procedures. *Aust. Ecol.* **26**, 535–546. (doi:10.1046/j.1442-9993.2001.01154.x)
95. Wright W, Vincent JF. 1996 Herbivory and the mechanics of fracture in plants. *Biol. Rev.* **71**, 401–413. (doi:10.1111/j.1469-185X.1996.tb01280.x)
96. Richter A, Boudinot B, Yamamoto S, Katzke J, Beutel RG. 2022 The first reconstruction of the head anatomy of a cretaceous insect, † *Gerontoformica gracilis* (Hymenoptera: Formicidae), and the early evolution of ants. *Insect Syst. Divers.* **6**, 1–80. (doi:10.1093/isd/ixac013)
97. Kang V, Püffel F, Labonte D. 2023 Three-dimensional kinematics of leafcutter ant mandibles: not all dicondylic joints are simple hinges. Figshare. (doi:10.6084/m9.figshare.c.6834890)